C.E. SACLAY
DSM

SERVICE D'ÉTUDE DES DÉTECTEURS

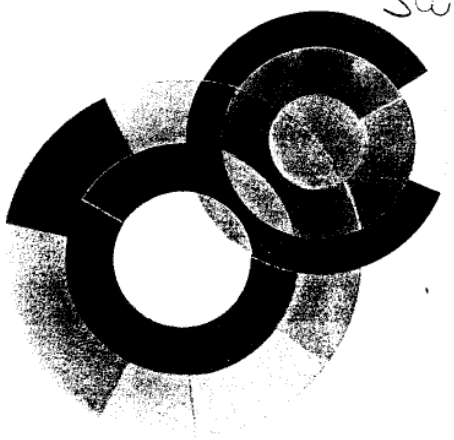

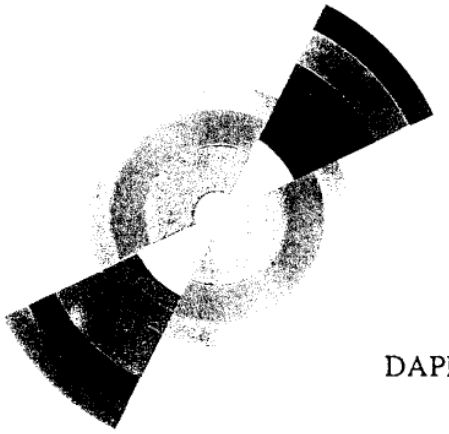

DAPNIA/SED 95-04 December 1995

MICROMEGAS: A HIGH-GRANULARITY POSITION-SENSITIVE GASEOUS DETECTOR FOR HIGH PARTICLE-FLUX ENVIRONMENTS

Y. Giomataris, Ph. Rebourgeard and J.P. Robert

G. Charpak

Submitted to Nuclear Instruments and Methods

DAPNIA

Le DAPNIA (**D**épartement d'**A**strophysique, de physique des **P**articules, de physique **N**ucléaire et de l'**I**nstrumentation **A**ssociée) regroupe les activités du Service d'Astrophysique (SAp), du Département de Physique des Particules Elémentaires (DPhPE) et du Département de Physique Nucléaire (DPhN).

Adresse : DAPNIA, Bâtiment 141
CEA Saclay
F - 91191 Gif-sur-Yvette Cedex

MICROMEGAS: a high-granularity position-sensitive gaseous detector for high particle-flux environments

Y. Giomataris, Ph. Rebourgeard and J.P. Robert

CEA/DSM/DAPNIA/SED-C.E-Saclay
91191 Gif/Yvette, France

G. Charpak

Ecole Superieure de Physique et Chimie Industrielle de la ville de Paris, ESP, Paris and CERN/AT, Geneva

ABSTRACT

We describe a novel structure for a gaseous detector that is under development at Saclay. It consists of a two-stage parallel-plate avalanche chamber of small amplification gap (100 μm) combined with a conversion–drift space. It allows a fast removal of positive ions produced during the avalanche development. Fast signals ($\leq$ 1 ns) are obtained during the collection of the electron avalanche on the anode microstrip plane. The induced positive ion signal has a rise time of 100 ns. The fast evacuation of positive ions combined with the high granularity of the detector provide a high rate capability. Gas gains of up to 10^5 have been achieved.

1 Introduction

Multiwire proportional chambers have been originally designed for high-rate applications[1]. Their flux capability was mainly limited by the positive-ion space charge created because of the low ion drift velocity with a typical drift time of several tenths of microseconds. Their spatial resolution was limited by the wire spacing, which was of the order of 1 mm.

To overcome these limitations, a new technique, the microstrip gas chamber (MSGC), has been developed over the last eight years[2, 3, 4]. Wires are replaced by strips printed on an insulating support; a high electric field region, sufficient for electron multiplication, is created between the thin cathode and anode conductive strips. It is a new class of gas detector relying on the microelectronics technology. The small inter-strip pitch allows a good spatial resolution, inferior to 100 μs and the fast collection of the charges offers the possibility to cope with higher counting rates. One limitation of the MSGC detector is the fact that the avalanche multiplication does not exceed 10^4, because of breakdown on the insulator surface. Positive ions created during the avalanche process and accumulated on the insulator, locally modify the electric field and cause a drop of the gain in the irradiated area of the detector[5]. A lot of effort has been invested, during the last few years, to resolve the charging-up problem by a careful choice of the resistivity of the substrate or a special treatment of its surface. Another type in this class of gas detectors, the micro-gap chamber[6], was recently developed aiming to resolve the charging-up problem and giving superior results in terms of rate capability and spatial resolution.

Another possible way out is the use of a special asymmetric configuration of the multiwire structure[7, 8] with alternating anodes and field-shaping wires, mounted close to the cathode plane with engraved pick-up strips orthogonal to the wire direction. The performance of this structure equals that of the MSGC in terms of rate capability and spatial resolution. In addition it can achieve higher electron multiplication factors and it operates in a stable fashion for long irradiation periods. The drawback here is the use of delicate wires and the wire stretching force, which is proportional to the total number of wires acting in the wire frame; this therefore has to be of substancial thickness.

In this paper we present a new approach where the wire plane is replaced by a thin electroformed micromesh. The amplification occurs between the mesh plane and the microstrip plane. A small gap, of about 100 μs, between the anode and cathode plane is kept by precise insulating spacers. The device operates as a two-stage parallel plate avalanche chamber and it is called MICROMEGAS (MICRO-MEsh-GAseous Structure).

2 Description of MICROMEGAS

It is a miniaturized version of a very asymmetric two-stage parallel plate detector. A micromesh separates the conversion space, of about 3 mm, from a small amplification gap that can be as small as 100 μm . This configuration allows us to obtain, by applying reasonable voltages in the three electrodes, a very high electric field in the amplification

region (about 100 kV/cm) and a quite low electric field in the drift region. Therefore, the ratio between the electric field in the amplification gap and that in the conversion gap can be tuned to large values, as is required for an optimal functioning of the device. Such a high ratio is also required in order to catch the ions in the small amplification gap: under the action of the high electric field, the ion cloud is quickly collected on the micromesh and only a small part of it, inversely proportional to the electric field ratio, escapes to the conversion region. Figure 1 shows a schematic representation of a typical detector. It consists of the following components:

1. Anode electrode. Anode strips of gold-coated copper of 150 μm , with 200 μm pitch, are printed on a 1 mm substrate. The thickness of the copper strip was 5 μm . Thinner strips were easily obtained by vacuum deposition. These allow a substantial reduction of the interstrip capacitance. Both metal-deposition techniques can be applied on a 50 μm thick Kapton substrate, whenever a reduction of the material of the detector is required. The strips were grounded through low-noise charge preamplifiers of high gain (4 V/pC).

2. Quartz fibres of 75 μm , with 2 mm pitch, were stretched and glued on a G10 frame. The quartz frame was then mounted on the strip surface, defining a precise (2%) gap. Thicker (150 and 230 μm) quartz spacers were also utilized during our tests.

3. The micromesh. Figure 2 is a photograph of the micromesh obtained with a microscope at a magnification of 100. It is a metallic grid, 3 μm thick, with 17 μm openings every 25 μm . It is made of nickel, using the electroforming technique, which is flexible and exhibits a high degree of fidelity of the electrodeposited layer. The use of the photographic process and especially high-resolution emulsions, enssures a high precision, better than 1 μm . The transparency was measured to be 45%.

4. The conversion-drift electric field was defined by applying negative voltages on the micromesh (HV2) and a slightly higher voltage on a second electrode (HV1), spaced by 3 mm in order to define a conversion–drift space. It was made by a standard nickel mesh, 100 μm thick, having 80% transparency, in order to allow an efficient penetration of the various radioactive sources used for the test and fixed on the top of the gross mesh. For the final detector, thin aluminized mylar can be used to define electrode HV1 and ensure at the same time the required gas tightness of the chamber.

5. The gas volume. The various elements of the parallel-plate structure were placed in a tight stainless steel vessel flushed by a standard gas mixture of Ar + 10% CH_4 at atmospheric pressure. A metallic holder was mounted on top of the parallel plate chamber to support the radioactive source and a stainless steel collimator 1 mm thick with a 2 mm hole. The metallic source holder can move horizontally and allow a rough scan of the active surface of the detector. Figure 3 shows a three-dimensional view of MICROMEGAS. The various elements of the detector are the drift electrode, the micromesh, the quartz spacers and the anode strips.

3 Electric-field configuration

Ionization electrons, created by the energy deposition of an incident charged particle in the conversion gap, drift and can be transferred through the cathode micromesh; they are amplified in the small gap, between anode and cathode, under the action of the electric field, which is high in this region. The electron cloud is finally collected by the anode microstrips, while the positive ions are drifting in the opposite direction and are collected on the micromesh. The electric field must be uniform in both conversion and amplification spaces. This is easily obtained by using the micromesh as the middle electrode. The electric-field shape is, however, disturbed close to the holes of the micromesh. The knowledge of the shape of the field lines close to the micromesh is a fundamental issue for the operation of our detector, and especially for the efficiency of the passage of electrons through the micromesh, as well as, for the fast evacuation of the positive-ion build-up.

In a first approximation the strip structure was neglected assuming a plane electrode. Hence, symmetry considerations lead to a model which is limited on a 1/8 of an elementary cell. The electrostatic potential follows Laplace's law $\Delta V=0$. In order to solve this equation, the CASTEM2000 software has been used. CASTEM2000 is usually employed for thermomechanical calculations. Since temperature follows Laplace's law, a useful analogy with the electrical potential can be made. Boundary conditions are deduced from the symmetry of the model. As no field-lines are leaving the cell, it is an adiabatic case, and the electrical potential is set on the three electrodes. Under the assumption that the field, far from the micro-mesh, is homogeneous, one can speed up the computer calculation in the vicinity of that electrode. In the appendix we give details of these calculations and of how the electron transmission, as well as the ion collection on the micromesh, is defined and computed. The results are given as a function of the parameter ξ, which is the ratio between the electric fields in the amplification and in the conversion regions.

Figure 4 describes the evolution of the field-line configuration for various values of the ratio ξ. For low values of ξ, most of the lines leaving the first electrode reach the micromesh. So, in that case the electron transmission is poor. For large values of ξ, which corresponds to the regular operation of the detector, most of the lines of the conversion field passing through the hole of the micromesh and reach directly the third anode electrode. In this case we reach a full electron transmission. On the other hand most of the lines on the anode plane end in the micromesh, so ions created during the avalanche process will be collected by the micromesh with a high efficiency. Figure 5 shows the electron and ion transmission through the micromesh. For large values of ξ, the electron transparency becomes 1, while the ion transmission is extremely low and becomes lower still for larger values of the ratio ξ. We would like to point out that the simulation shows that the optical transparency of the micromesh is not a fundamental issue, since electrons can be transmitted by applying higher field ratio.

4 Laboratory tests

4.1 Microgrid electron transmission measurement

In a separate set-up we have tested the validity of the simulation model. The electroformed micromesh (HV2) was placed between two electrodes at a distance of 5 mm to define two gaps, both operating in the ionization chamber mode. A ^{254}Cf radioactive source is placed on top of one of the electrodes (HV1). Each fission creates several millions of primary electrons in the gas mixture, a signal detectable by our high-gain charge preamplifiers. The electron cloud is created near the top electrode; through the action of the electric field applied in this gap, it drifts to the middle electrode, the micromesh, giving a signal S1. Part of the electron cloud can be transmitted to the second gap when an electric field is applied there , giving a signal S2. The transmission is defined as the ratio between the two signals η=S1/S2. We have studied the electron transmission trough the micromesh for various electric fields applied on the two gaps. Figure 6 shows the electron transmission as a function of the ratio of the two electric fields: ξ=E2/E1. There is a fast rise up to a ratio of about 10; then a slower rise up to a ratio 40; finally a plateau when the full electron cloud is transmitted through the micromesh. This is a particular behaviour, which characterizes the micromesh, and it is different from the measurements obtained with conventional wiremeshes having larger holes. At a first order, the agreement with our simulation model is satisfactory.

4.2 Operation at high gain

A prototype similar to the one described in section 2, has been exhaustively tested. Most of the measurements were performed by using an amplification gap of 140 μm . Since anode strips were grounded, a negative voltage was applied on the micromesh HV2 and a slightly more negative voltage on the drift electrode HV1. Under these conditions electrons produced by the radioactive source in the conversion gap were easily transferred to the amplification gap through the fine grid. Comfortable signals were obtained by irradiating the detector with ^{241}Am source. The rise-time of the signal was about 200 ns, corresponding to the drift of the ion cloud produced during the avalanche process. With a smaller gap of 75 ns, the rise-time was inferior to 100 ns as is shown in Figure 7. Obviously after that lapse of time, ions produced in the avalanche, which can disturb the electric field, are fully evacuated from the detector; it is therefore possible to detect a second particle entering the same area. It gives a substantial improvement in terms of rate capability over conventional gaseous detectors. We were able to observe fast signals due to the collection of the electron cloud in the anode. Figure 8 shows such a signal taken through a fast current preamplifier. The rise-time is 4 ns and it is a convolution of the physical effect itself, the rise of the amplifier and the effect of the capacitance of the channel.

We have studied the dependence of the proportional gain of the detector on the cathode voltage, using the ^{241}Am source at low gains and ^{55}Fe at higher gains. Figure 9 shows the measured gain variation, as a function of the applied voltage, using the 140 μm amplification gap and a gas mixture of Ar + (10%) CH4 at atmospheric pressure. It can be seen that gains close to 10^5 could be safely reached. Notice that, using

more adequate quenchers, superior gains must be achieved. At those gain values single electron detection is possible and therefore it could be possible to reduce the conversion gap to 2 mm or even to 1 mm, using a heavier gas. Reducing the conversion gap one can reduce the parallax error for inclined tracks and improve the spatial resolution.

The energy resolution of the detector was measured using the ^{55}Fe radioactive source. The obtained pulse-height distribution is shown in Figure 10. One can easily separate the 5.9 keV peak and the Ar escape peak at 3.5 keV. The energy resolution obtained, 22% (FWHM), is satisfactory. It shows that the detector can achieve a reasonable homogeneity of the gain, in spite of possible fluctuations due to mechanical misalignments inside the micro-amplification gap. Long-term gain-stability measurements have not been performed. But we can point out that we observed no notable effect of charge-up or drop of the gain during our tests. Stability of gain and simple low-cost construction of the detector could be a considerable advantage of this detector compared to the MSGC.

5 Conclusion - Outlook

These results indicate that our detector combines most of the qualities required for a high-rate position-sensitive particle detector: Excellent resolution can be obtained with fine strips printed on a thin G10 substrate or a thin kapton foil. For this purpose, a conventional low-cost technology is sufficient and the connection to the electronic chain is straight-forward. We are also considering incorporation of part of the electronics on the substrate, using the same technology, to further simplify the construction of a large detector. The study of the electron transmission though the micromesh looks quite promising. Under reasonable electric field values applied on the conversion and the amplification gap, the electron cloud is fully transmitted to the amplification region. A model simulating the electric field inside the detector has been developed. The agreement with the experimental data is quite reasonable. High gain in steady operation has been achieved. At such gain, high efficiency can be obtained for minimum-ionizing particles with excellent signal-to-noise ratio. Reduction of the conversion gap to 2 mm or to 1 mm can be envisaged in order to reduce the radiation length and the parallax error induced by inclined charged particles. This would also improve the spatial resolution. The fast evacuation of the ion space charge and the high granularity of the detector open the way to the achievement of very high counting rates, beyond 10^6 particles/mm^2/s. Using conventional charge preamplifiers with long picking time, the total rise-time is of the order of 100 ns, which corresponds to the total ion drift time, without any shaping of the signal. In some applications it can be envisaged to use fast current preamplifiers with time constants of the order of 1 ns to catch the electron signal. The device is simple, easy to operate, and cost-effective.

6 Appendix

The model used, simulating the electric-field configuration near the micromesh, can be represented with a set of three parameters, ξ, η and f, where ξ is the ratio of the electric field in the avalanche gap to the field in the conversion gap, η is the optical

transparency of the micromesh and f is a form factor set to the ratio of the mesh width to the mesh pitch.

The calculation provides directly the electrostatic potential V in the cell and the electric field is given by E=-gradV. The flows in the three electrodes are $\phi 1$, $\phi 2$ and $\phi 3$ respectively, they can be deduced by the formula $\phi = \int E.dS$. In order to find the electronic transparency it is useful to express $\phi 1$, $\phi 2$ and $\phi 3$ in terms of partial flows between two electrodes $\phi 13$, $\phi 12$ and $\phi 23$ as it is illustrated on Figure 11. The quantities are related by

$$\begin{aligned} \phi 1 &= \phi 13 + \phi 12 \\ \phi 2 &= \phi 23 - \phi 12 \\ \phi 3 &= -\phi 13 + \phi 23 \end{aligned} \tag{1}$$

in agreement with $\phi 1 + \phi 2 + \phi 3 = 0$. The electronic transparency is given by

$$\eta_e = \frac{\phi 13}{\phi 13 + \phi 12} \tag{2}$$

and is a function of ξ, η and f. The ion transparency, supposing a diffusion process, can be expressed as :

$$\eta_i = \frac{\phi 13}{\phi 13 + \phi 23} \tag{3}$$

Symmetry considerations between the two gaps separated by the micromesh lead to the conclusion that η_i and η_e are not independant and can be related by :

$$\eta_i(\xi, \eta, f) = \eta_e(\frac{1}{\xi}, \eta, f) \tag{4}$$

Acknowledgements

We are grateful to many colleagues for their continuous support and help. J. Haissinski the director of our department and P. Micolon the director of the detector development group, unfailing encouraged us to persist. We would like to thank J. P. Passerieux and O. Mayard for providing low noise preamplifiers. We are indebted to P. Mangeot and C. Mazur for many fruitful discussions. The authors wish to thank A. Giganon, C. Jeanney, D. Zacharian and Y. Piret for their technical assistance. We would like also to thank S. Vascotto for her competent help in reading and correcting this paper. Finally we would like to thank Catherine Allegrini and Francois Voltaire for the acronym.

References

[1] G. Charpak, R. Bouclier, T.Bressani, J. Favier and C. Zupancic, Nucl. Instr. Meth. 62(1968)235

[2] A. Oed, Nucl. Instr. Meth. A263(1988)351

[3] F. Angelini, R. Bellazzini, A. Brez, M.M. Massai, G. Spandre and M.R. Torquati, Nucl. Instr. Meth. A283(1989)69

[4] R. Bouclier, J.J. Florent, J. Gauden, G. Million, A. Pasta, L. Ropelewski, F. Sauli and L. I Shekhtman, Nucl. Instr. Meth. A323(1992)236.

[5] S.F. Biagi, J.N. Jackson, T.J Jones and S. Taylor, Nucl. Instr. Meth. A323(1992)258

[6] F. Angelini, R. Bellazzini, A. Brez, M.M. Massai, R. Raffo, G. Spandre and M.A. Spezzina, Nucl. Instr. Meth. A335(1993)69

[7] G. Charpak, I. Crotty, Y. Giomataris, L. Roppelewski and C. Williams, Nucl. Instr. Meth. A346(1994)506

[8] E. Roderburg et al., Nucl. Instr. Meth. A323(1992)140

Figure Captions

Figure 1. A schematic view of Micromegas: the 3 mm conversion gap and the amplification gap separated by the micromesh and the anode strip electrode.

Figure 2. A photograph of the micromesh using a microscope.

Figure 3. A three dimensional view of the detector elements.

Figure 4. Field configuration for various ξ ratios.

Figure 5. Calculated electron and ion transparency

Figure 6. Measured electron transmission through the micromesh for various values of the ξ ratio

Figure 7. Signal seen on the anode by a charge preamplifier. The rise-time reflects the ion cloud collection.

Figure 8. Fast signal measured on the anode using a fast-current preamplifier.

Figure 9. Variation of gas-gain with anode voltage. The gas mixture was Ar + (10%) CH4 at atmospheric pressure.

Figure 10. Pulse-height distribution from an ^{55}Fe source. The position of the 5.9 keV peak corresponds to a gas gain of 2000.

Figure 11. Electric field configuration and partial flows

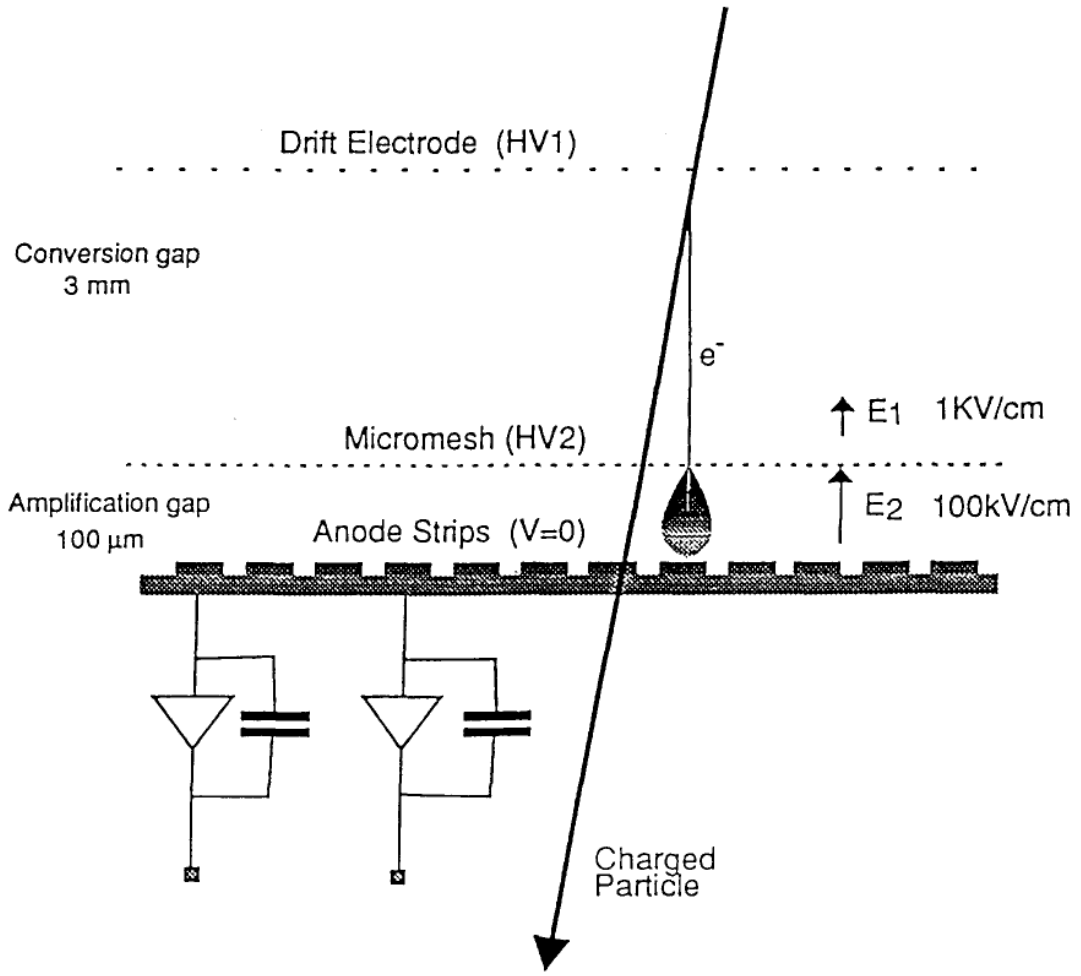
Drift Electrode (HV1)
Conversion gap
3 mm
e⁻
E1 1KV/cm
Micromesh (HV2)
Amplification gap
100 μm
E2 100kV/cm
Anode Strips (V=0)
Charged
Particle

Fig. 1

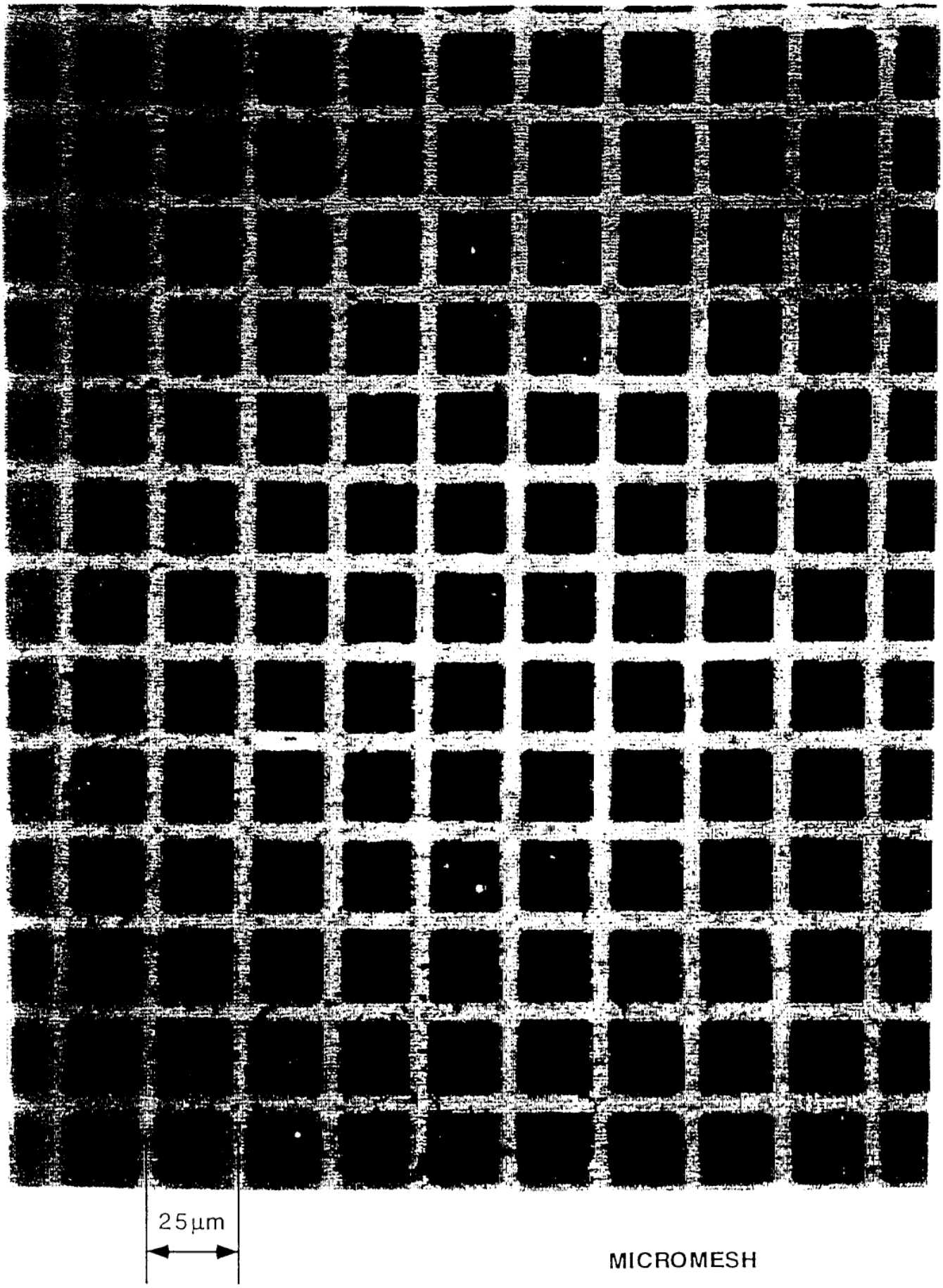

Fig. 2

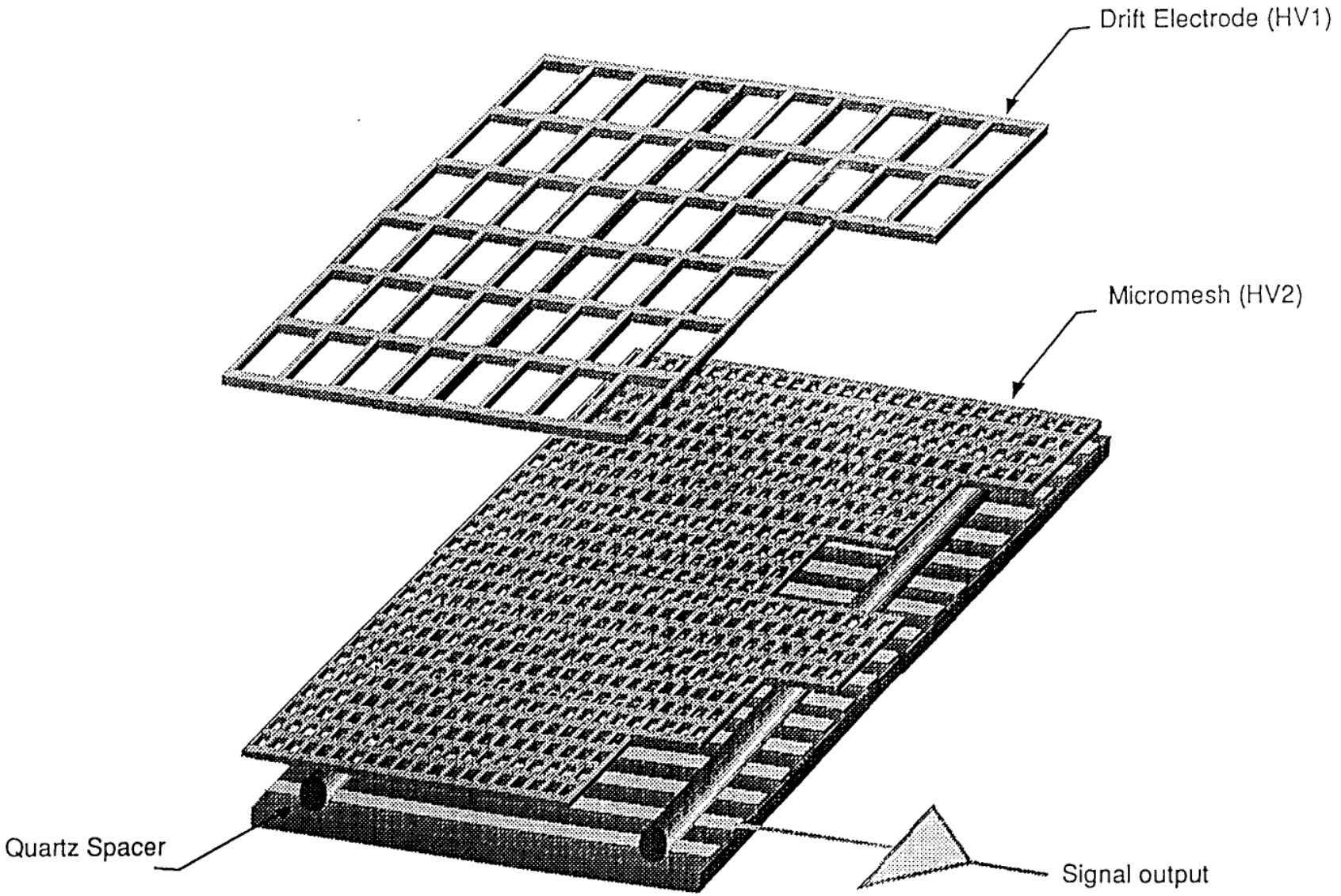
Drift Electrode (HV1)
Micromesh (HV2)
Quartz Spacer
Signal output

Fig. 3

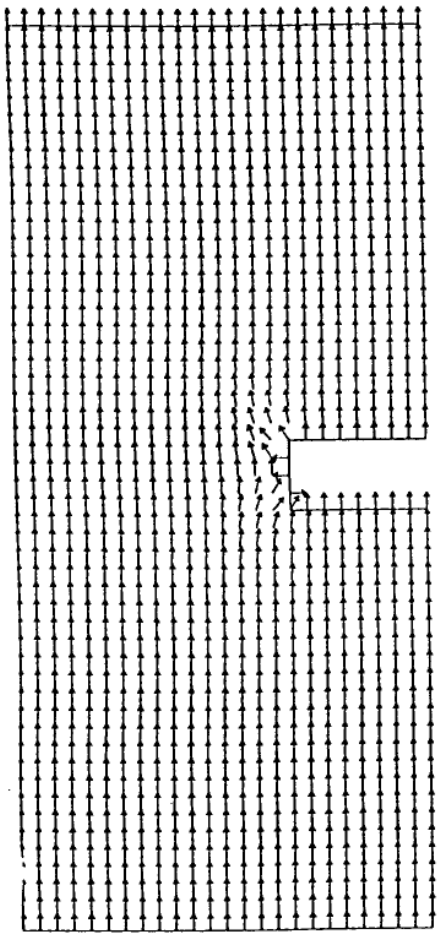

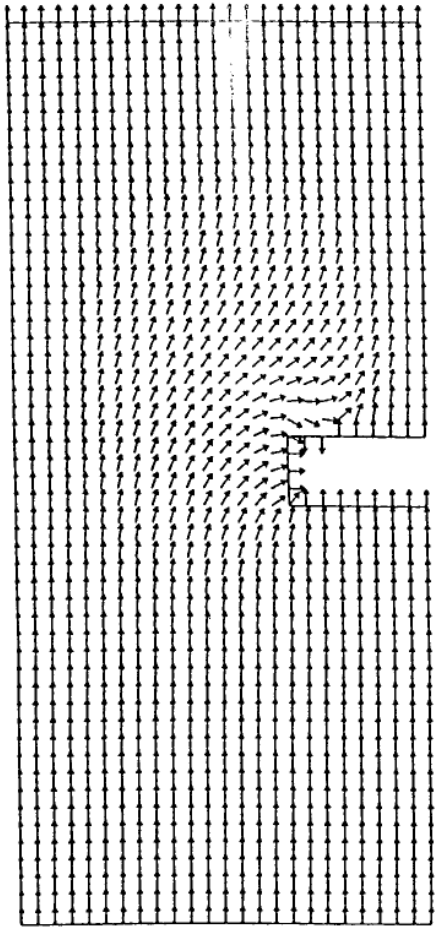

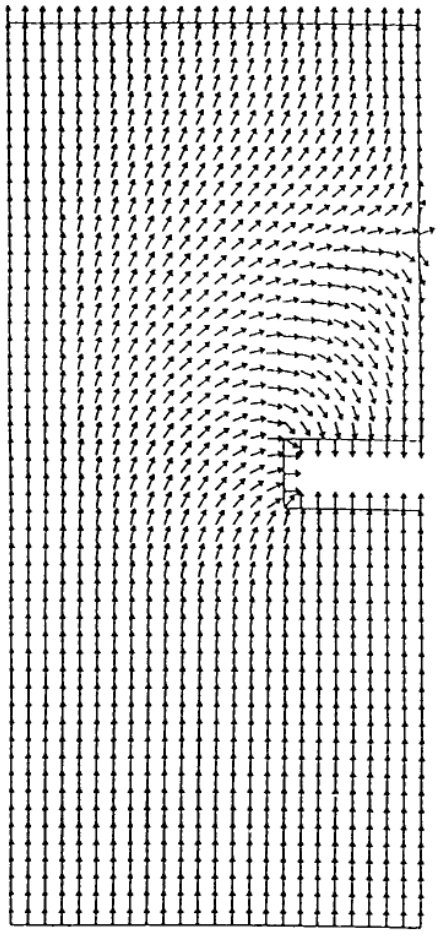

Fig. 4

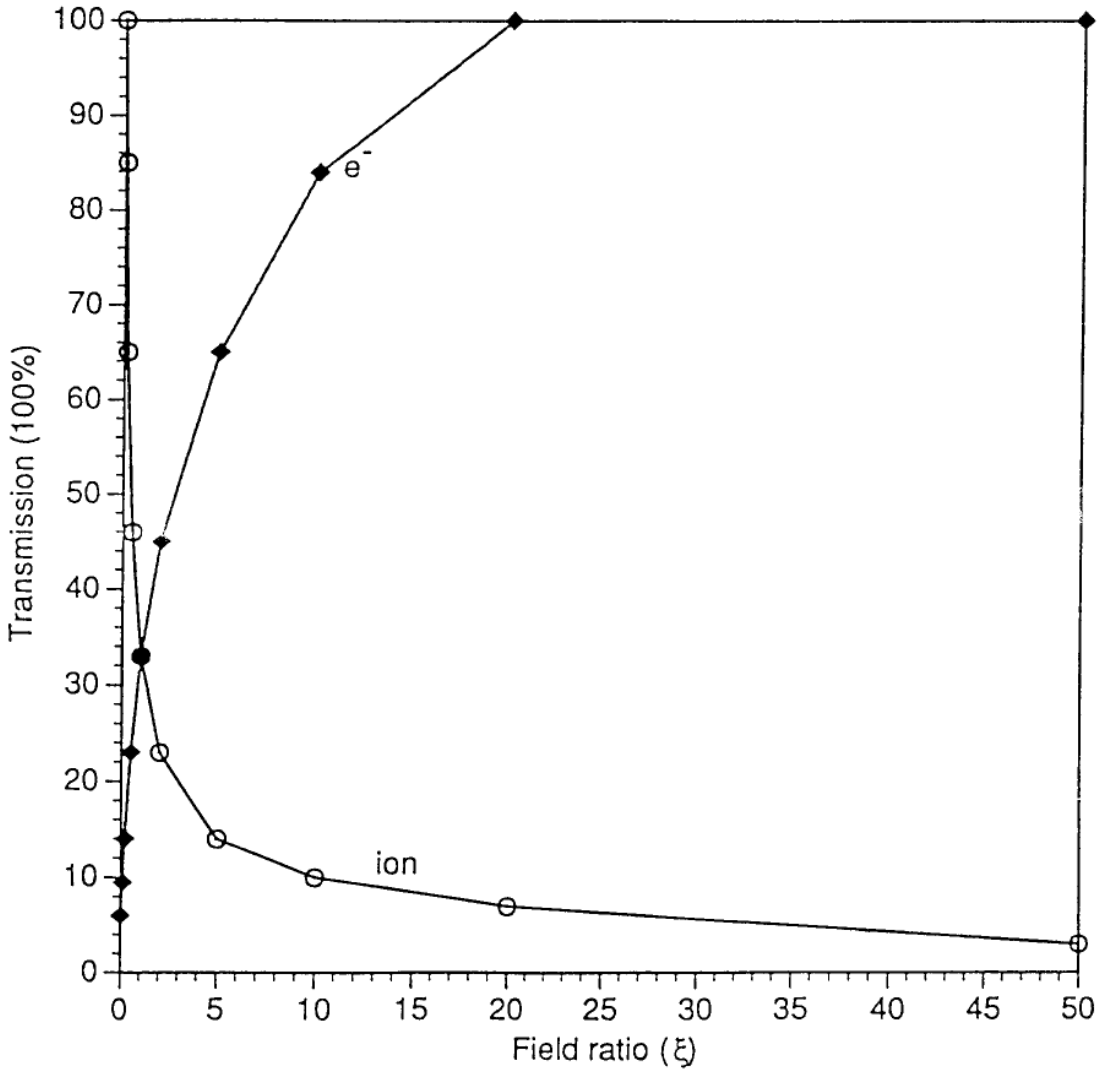
Transmission (100%)
Field ratio (ξ)
e⁻
ion
0
10
20
30
40
50
60
70
80
90
100
0
5
10
15
20
25
30
35
40
45
50

Fig. 5

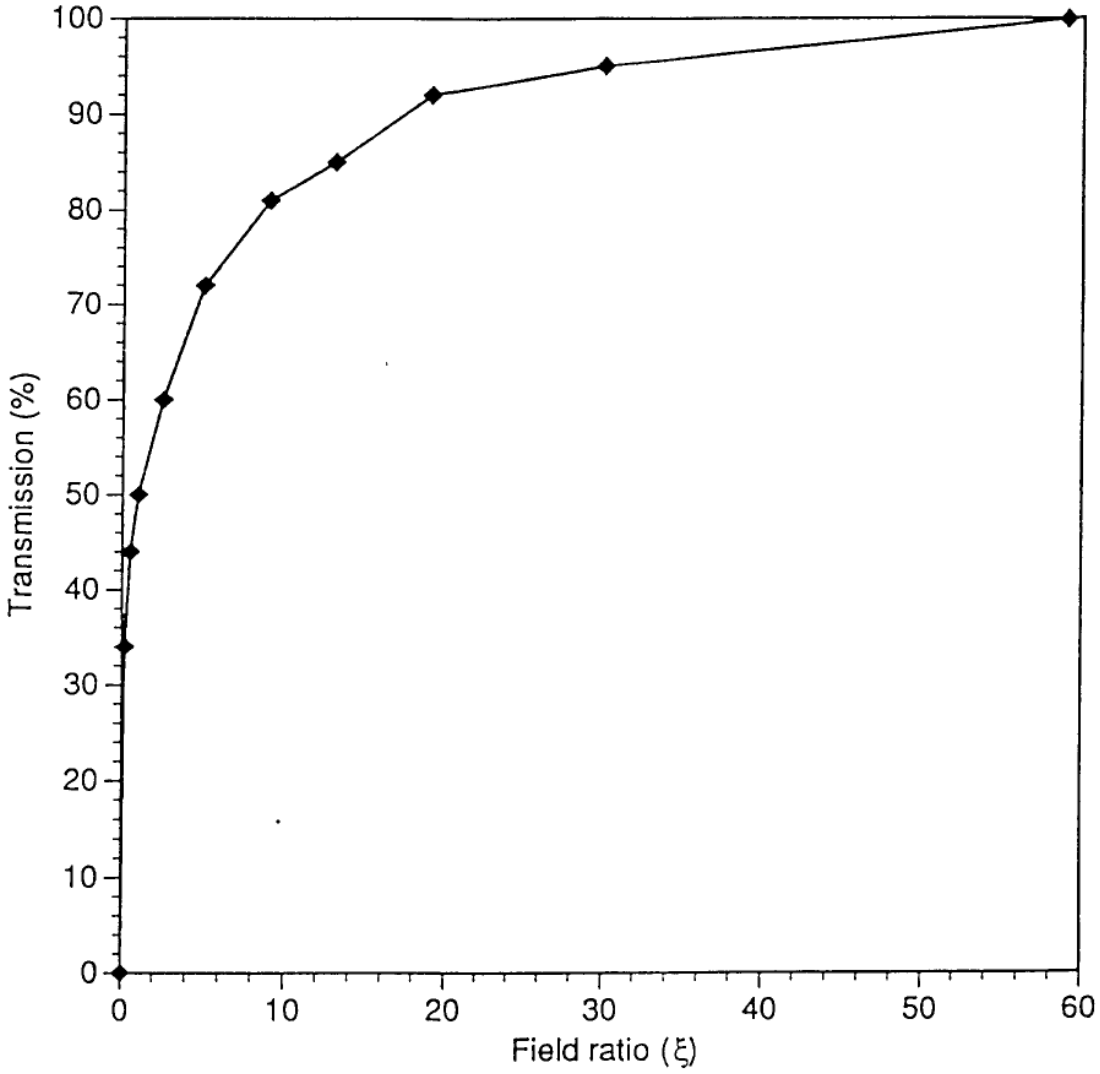
Transmission (%)
100
90
80
70
60
50
40
30
20
10
0
0
10
20
30
40
50
60
Field ratio (ξ)

Fig. 6

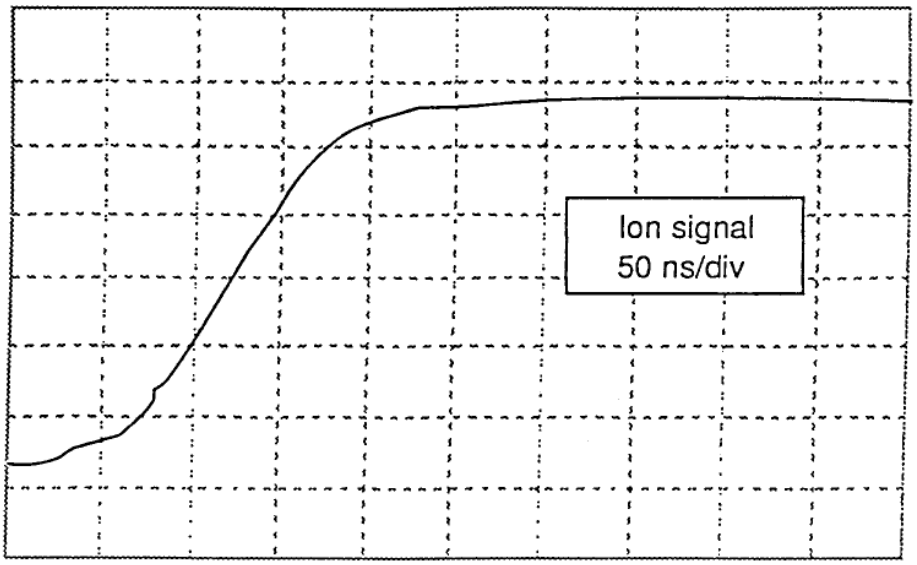

Fig. 7

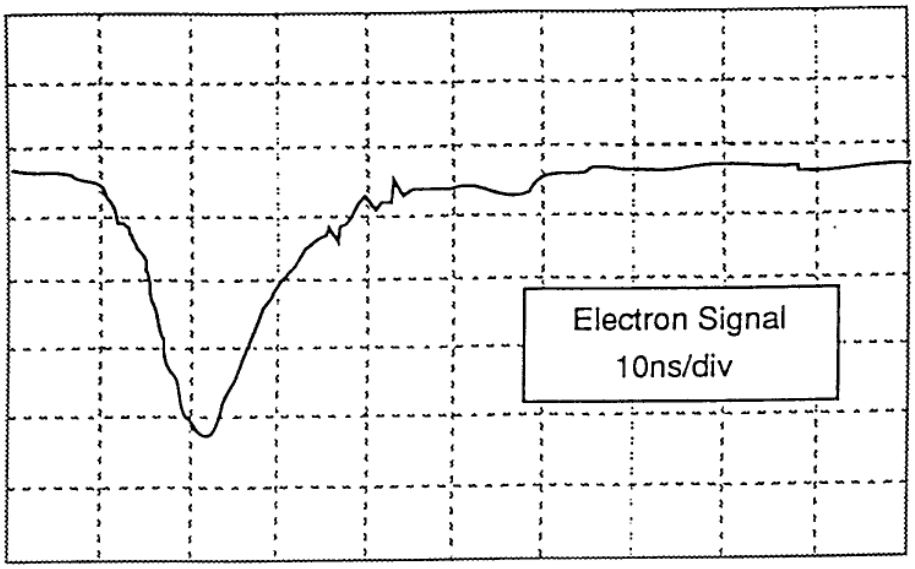

Fig. 8

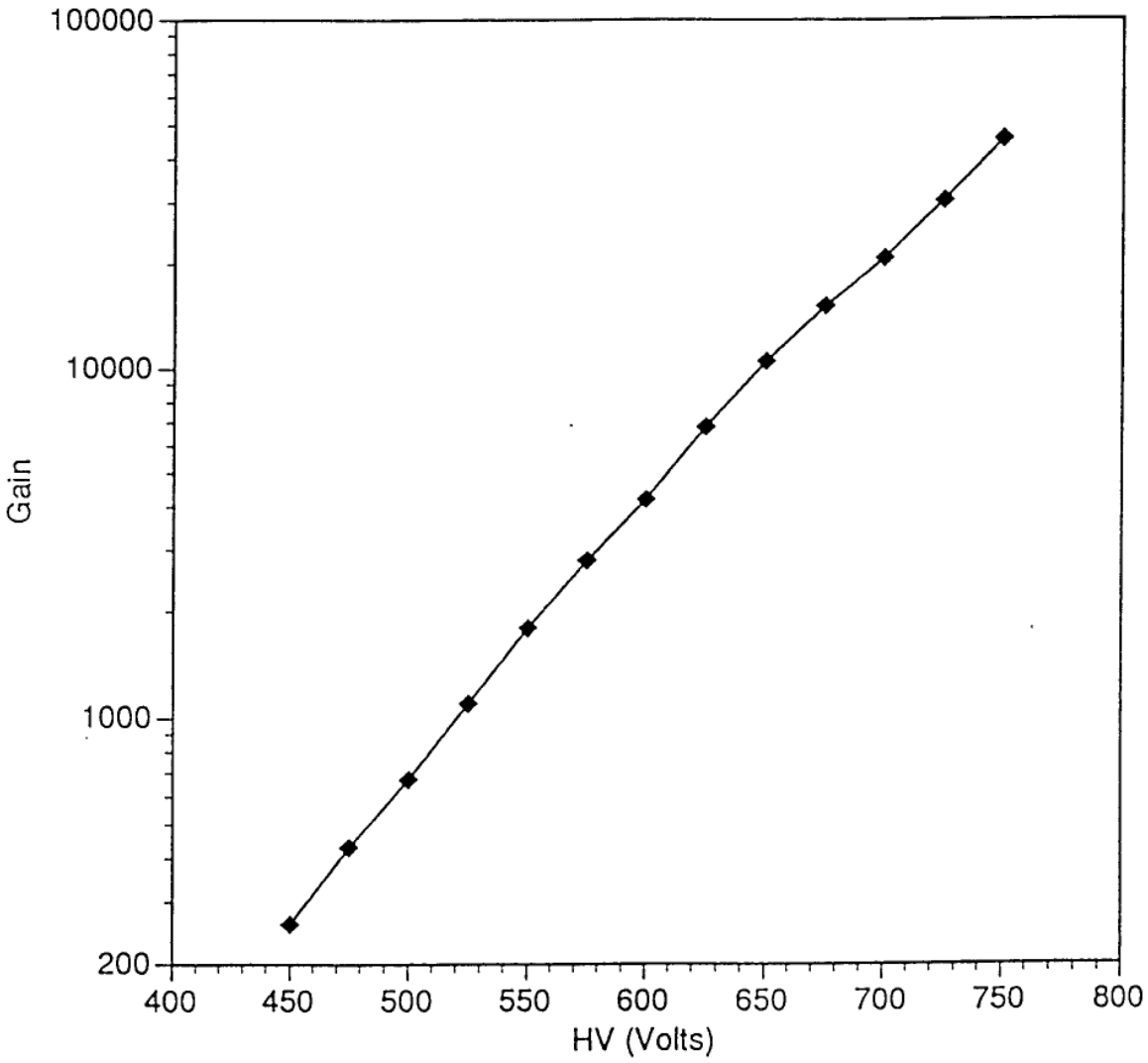
100000
10000
1000
200
Gain
400
450
500
550
600
650
700
750
800
HV (Volts)

Fig. 9

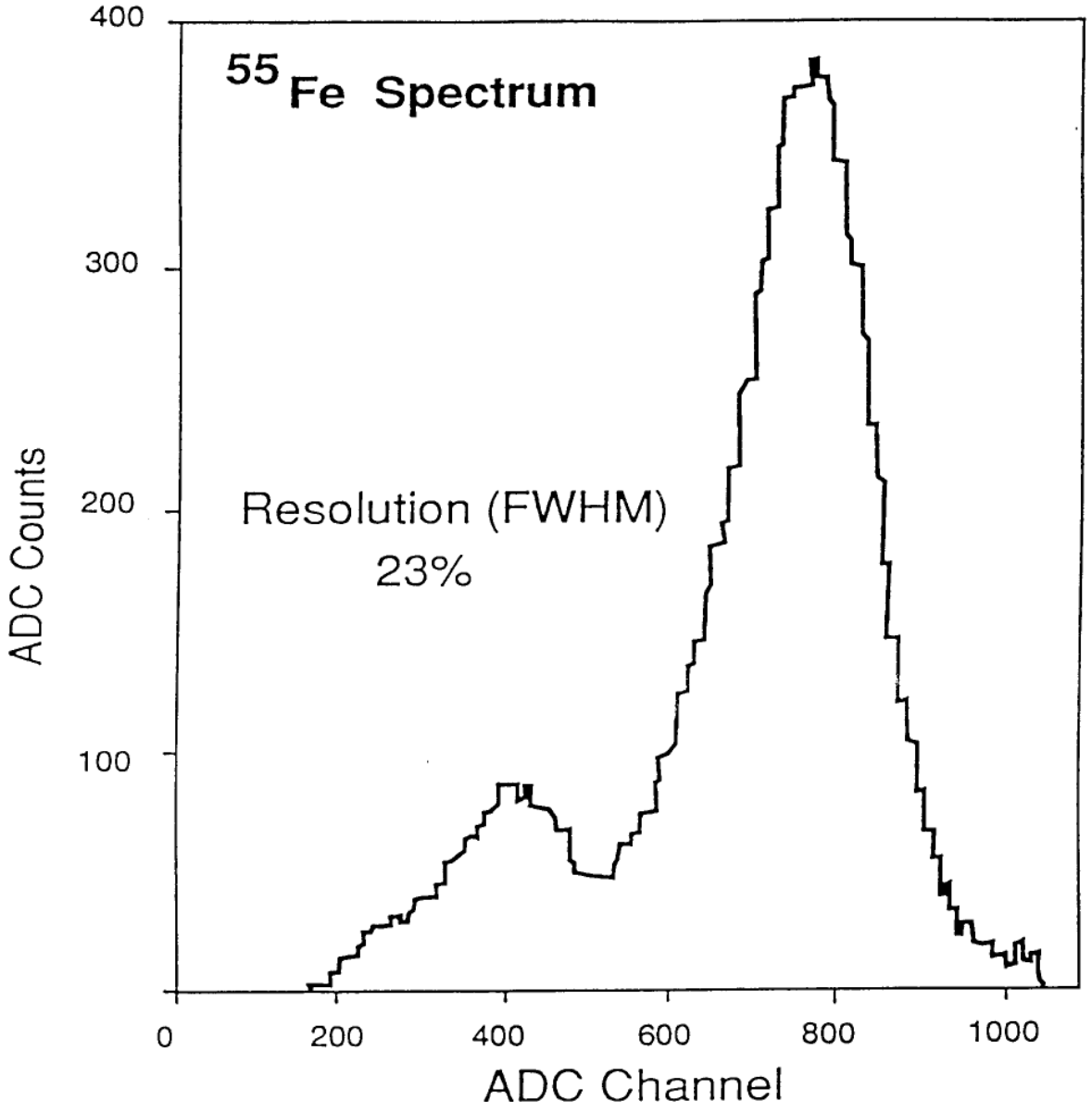
55 Fe Spectrum
Resolution (FWHM)
23%
ADC Counts
ADC Channel
400
300
200
100
0
200
400
600
800
1000

Fig. 10

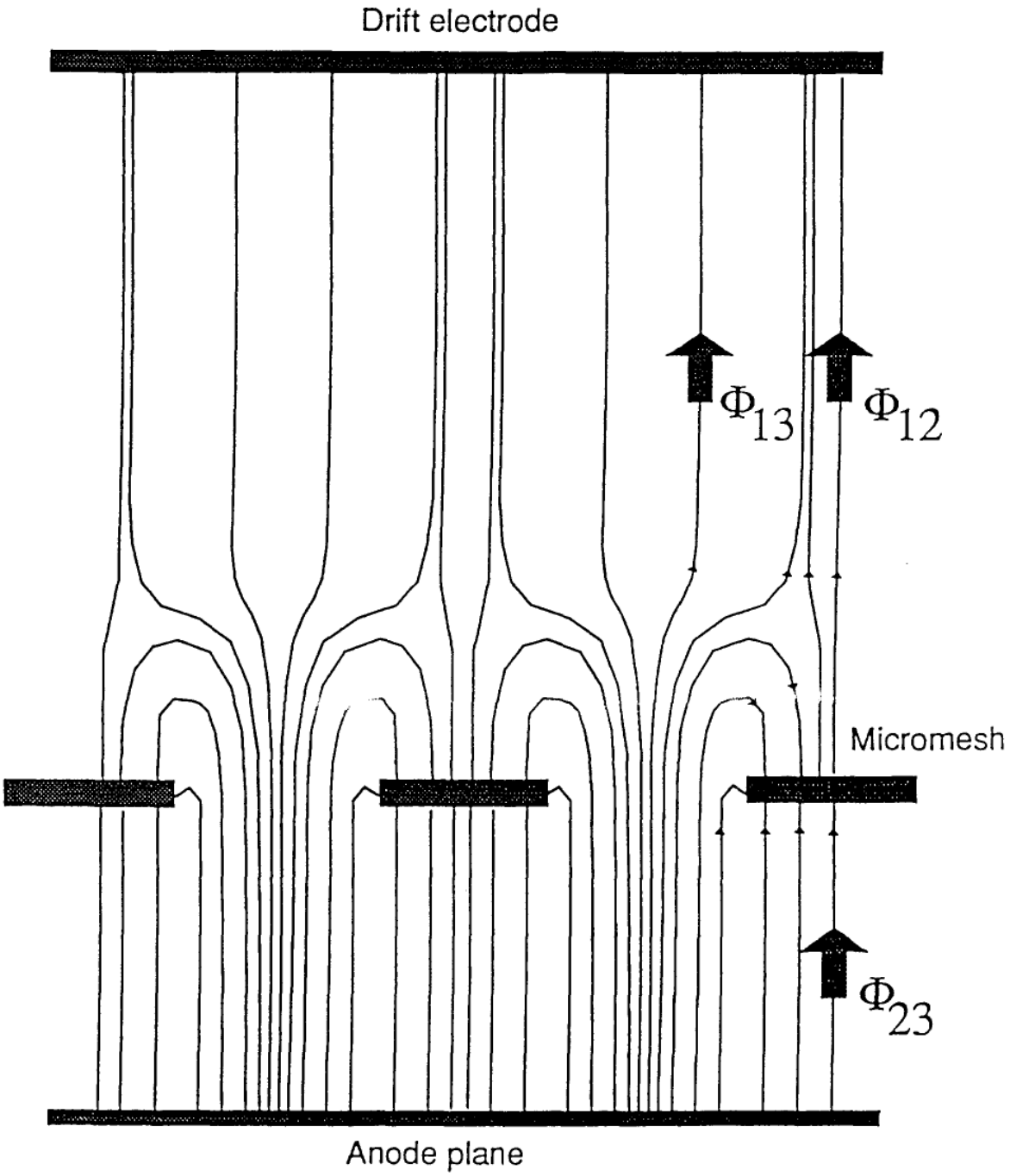

Fig. 11